American Journal of Mechanics and Applications
2016; 3(5): 42-55
http://www.sciencepublishinggroup.com/j/ajma
doi: 10.11648/j.ajma.20150305.12
ISSN: 2376-6115 (Print); ISSN: 2376-6131 (Online)

Influence of an Inclined Magnetic Field on Peristaltic Transport of Pseudoplastic Nanofluid Through a Porous Space in an Inclined Tapered Asymmetric Channel with Convective Conditions

Ali M. Kamal, Ahmed M. Abdulhadi

College of Science, University of Baghdad, Baghdad, Iraq

Email address:
alikammal@yahoo.com (A. M. Kamal), ahm6161@yahoo.com (A. M. Abdulhadi)

To cite this article:
Ali M. Kamal, Ahmed M. Abdulhadi. Influence of an Inclined Magnetic Field on Peristaltic Transport of Pseudoplastic Nanofluid Through a Porous Space in an Inclined Tapered Asymmetric Channel with Convective Conditions. *American Journal of Mechanics and Applications*. Vol. 3, No. 5, 2016, pp. 42-55. doi: 10.11648/j.ajma.20150305.12

Received: August 28, 2016; **Accepted**: September 9, 2016; **Published**: October 10, 2016

Abstract: The problem of peristaltic transport of a pseudoplastic nanofluid through a porous medium in a two dimentional inclined tapered asymmetric channel has been made. Convective conditions of heat and mass transfer are employed. The problem has been further simplified with the authentic assumptions of long wavelength and small Reynold's number. The governing equations for the balance of mass, momentum, temperature and volume fraction for pseudoplastic nanofluid are formulated. Effect of involved parameters on the flow characteristics have been plotted and examined.

Keywords: Pseudoplastic Nanofluid, Peristaltic Transport, Inclined Tapered Asymmetric Channel, Convective Conditions, Inclined Magnetic Field

1. Introduction

Peristaltic pumping is a form of fluid transport which is achieved via a progressive wave of contraction or expansion which propagates along the length of a distensible tube containing fluids. In general, this pumping takes place from a region of lower pressure to higher pressure. It is an inherent property of many of the smooth muscle tubes such as the gastrointestinal tract, male reproductive tract, fallopian tube, bile duct, ureter and oesophagus. The principle of peristaltic transport is also exploited in many industrial applications. These include sanitary fluid transport, transport of corrosive fluids, blood pumps in heart lung machines, novel pharmacological delivery systems etc. Since the experimental work of Latham [1], many investigations [2-4] dealing with peristaltic flow for different flow geometries and under various assumptions, have been presented by employing analytical, numerical and experimental approaches. Fung and Yih [2], who presented a model on peristaltic pumping using a perturbation technique, associated reflux with net backward flow. Barton and Raynor [3] studied the peristaltic motion in a circular tube by using the long wavelength approximation for intestinal flow. Shapiro et al. [4] extended their work for the steady flow of Newtonian fluids through the channel and tube with sinusoidal wall propagation and theoretically evaluated the reflux and trapping phenomena. The fluids present in the ducts of a living body can be classified as Newtonian and non-Newtonian fluids based on their shear-stress strain behavior. Further the peristalsis subject to magnetic field effects are significant in magnetotherapy, hyperthermia, arterial flow, cancer therapy, etc. The controlled application of low intensity and frequency pulsating fields modify the cell and tissue. Magnetic susceptible of chime is also satisfied from the heat generated by magnetic field or the ions contained in the chime. The magnets could heat inflammations, ulceration and several diseases of bowel (intestine) and uterus. Also biomechanical engineer has proved now that rheological properties are important in the industrial and physiological processes. The non-Newtonian fluids deviate from the classical Newtonian linear relationship between the shear stress and the shear rate. Due to complex rheological properties it is difficult to suggest a single model which exhibits all properties of non-

Newtonian fluids. Various models of non-Newtonian fluids are proposed. Abd-Alla et al. [5] discussed the effect of radial magnetic field on peristaltic transport of Jeffrey fluid in cylindrical geometry. Abd-Alla et al. [6] also discussed the influence of rotation and initial stresses on peristaltic flow of fourth grade fluid in an asymmetric channel. The peristaltic flow of nanofluid through a porous medium with mixed convection is analyzed by Nowar [7]. Kothandapani and Prakash [8] studied the combined effects of radiation and magnetic field on peristaltic transport of nanofluid. The studies related to peristalsis with heat and mass transfer for Newtonian fluid have been structured in refs. [9, 10]. Shaban and Abou Zeid [11] investigated the peristalsis between two coaxial cylinders when inner tube is rigid and outer flexible. Heat transfer is also considered in the study. Kothandapani and Prakash [12] Modeled the peristaltic flow of hyperbolic tangent nanofluid in an asymmetric channel with inclined magnetic field. Influence of convective conditions on peristaltic transport of non-Newtonian fluids under different flow situations are discussed in refs. [13, 14]. Ellahi et al. [15] studied the peristalsis in non-uniform rectangular duct with heat and mass transfer effects. Hayat et al. [16] discussed the peristaltic flow in a vertical channel filled with nanofluid by considering Soret and Dufour effects. Peristaltic transport of fourth grade fluid with convective conditions is numerically discussed by Mustafa et al. [17]. Effects of variable viscosity on peristalsis in the presence of magnetic field is studied by Abbasi et al. [18]. Kothandapani and Prakash [19] analyzed the peristaltic transport of nanofluid with thermal radiation and magnetic field in a tapered channel. Mehmood et al. [20] considered the partial slip effects on peristaltic transport in a channel with heat and mass transfer effects. Mathematical analysis has been carried out in the presence of magnetic field. In all of the above mentioned studies lubrication approach has been utilized to simplify the problems. It is seen that heat transfer in peristalsis has pivoted role. Specifically suchan effect is useful in the cancer therapy, hyperthermia, oxygenation and hemodialysis.

The study of nanofluids has become a subject of much interest in near past due to its wide range of applications in engineering, medicine and biochemistry. Choi [21] was the first who used the term nanofluid which refers to a fluid containing nanometer-sized particles. It further represents a liquid suspension containing ultra-fine particles that have diameters less than 50nm. These particles could be found in the metals such as (Al,Cu), oxides (Al2O2), carbides (SiC), nitrides (SiN) or nonmetals (graphite, car-bon nanotubes, droplets, nanosheets, and nanofibers). Tripathi and Beg [22] studied the impact of nanofluid characteristics for peristaltic motion in axisymmetric channel. Shehzad et al. [23] made a comparative study for the peristaltic transport of water based nanofluids. Abbasi et al. [24] studied the mixed convective peristaltic transport of nanofluid in presence of Joule heating and magnetic field. Hina et al. [25] investigated the peristaltic trans port of pseudoplastic fluid in a curved channel under the effects of heat/mass transfer and wall properties. No doubt the pseudoplastic fluid falls in the category of non-Newtonian fluids. Pseudoplastic fluid is a fluid whose apparent viscosity decreases with an increase in shear stress. They are often called shear-thinning fluids. Common examples of pseudoplastic fluids are ketchup, nail polish, molasses, whipped cream, paper pulp in water, ice, latex paint, some silicone oils, blood, some silicone coatings, etc. The peristaltic flow of pseudoplastic fluid in a curved channel under the influence of radial magnetic field has been investigated by Hayat et al. [26]. Recently, Hayat et al. [27] discussed the peristaltic flow of a pseudoplastic nanofluid in a tapered asymmetric channel under the influence of convective conditions.

The purpose of the present paper is to discuss the peristaltic flow of a pseudoplastic nanofluid in the inclined tapered asymmetric channel. To the best of authors knowledge, the idea of nanofluids in peristaltic flow problem under the effect of inclined magnetic field and porous space in the inclined tapered asymmetric channel has not been discussed so far. The governing equations of motion, energy of nanoparticles for pseudoplastic nanofluids have been carried out under the assumption of longwave-length and low Reynolds number. The reduced equations are then solved analytically and numerical computation has also been performed for the average rise in pressure. The effect of physical parameters such as non-uniform parameter, phase difference, Hartmann number, permeability parameter, Brownian motion parameter, thermophoresis parameter, Prandtl number, Eckert number, Froude number, Brinkman number are shown and discussed in detail with the help of graphs.

2. Mathematical Model

The constitutive equation for the wall geometry (see Fig. 1). A uniform magnetic field $\mathbf{B}=(B_0 \sin\vartheta, B_0 \cos\vartheta)$ is applied. The induced magnetic field is neglected by assuming a very small magnetic Reynolds number. Due to propagation of a train of waves may be defined thus:

$$H_1(X,t') = -d - \mathrm{m'X} - \mathrm{a_1}\sin\left[\frac{2\pi}{\lambda}(X-ct')+\phi\right], \text{ lower wall (1)}$$

$$H_2(X,t') = d + \mathrm{m'X} + \mathrm{a_2}\sin\left[\frac{2\pi}{\lambda}(X-ct')\right], \text{ upper wall (2)}$$

where a_1 and a_2 are the amplitudes of lower and upper walls, d is the half-width of the channel, λ the wavelength, m'(1) the non-uniform parameter of the tapered asymmetric channel and ∅ denotes the phase difference which varies in the range $0 \le \emptyset \le \pi$. Further $\emptyset = 0$ corresponds to symmetric channel with waves out of phase, i.e., both walls move outward or inward simultaneously. Also a_1 and a_2, d and ∅ satisfy the condition

$$a_1^2 + a_2^2 + 2a_1a_2d\cos(\emptyset) \le (2d)^2 \qquad (3)$$

The temperature and constration at the upper and lower

walls are assumed to be T_0, C_0 and T_1, C_1 respectively. The governing equations for the balance of mass, momentum, nano-particle temperature and volume fraction for an incompressible magnetohydrodynamic(MHD) pseudoplastic nanofluid are

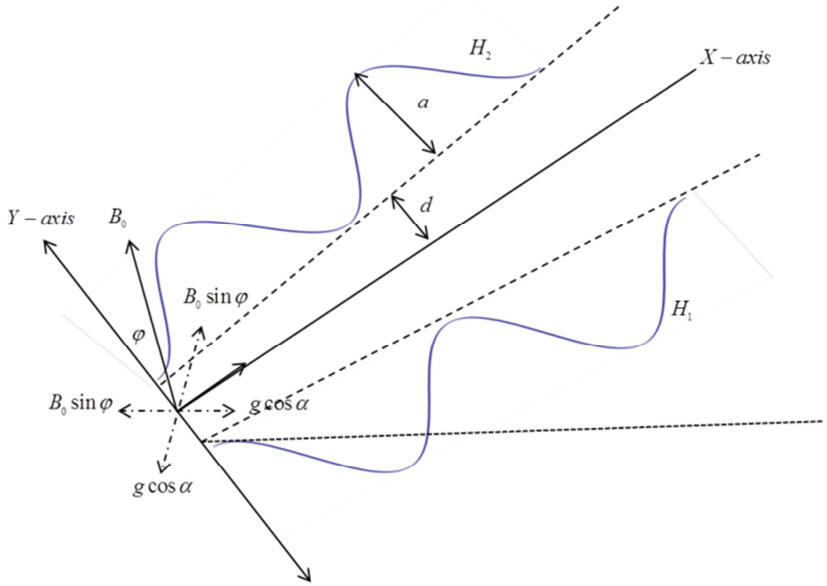

Fig. 1. *A physical sketch of the problem.*

$$\rho_f\left[\frac{\partial U}{\partial t'}+U\frac{\partial U}{\partial X}+V\frac{\partial U}{\partial Y}\right]=-\frac{\partial P}{\partial X}+\frac{\partial}{\partial X}(S_{XX})+\frac{\partial}{\partial Y}(S_{XY})+\sigma' \mathrm{B}_0^2\cos\vartheta(U\cos\vartheta-V\sin\vartheta)-\frac{\mu}{k}U+\rho g\sin\alpha, \tag{5}$$

$$\rho_f\left[\frac{\partial V}{\partial t'}+U\frac{\partial V}{\partial X}+V\frac{\partial V}{\partial Y}\right]=-\frac{\partial P}{\partial Y}+\frac{\partial}{\partial X}(S_{XY})+\frac{\partial}{\partial Y}(S_{YY})+\sigma' \mathrm{B}_0^2\sin\vartheta(U\cos\vartheta-V\sin\vartheta)-\frac{\mu}{k}V-\rho g\cos\alpha, \tag{6}$$

$$(\rho c')_f\left[\frac{\partial T}{\partial t'}+U\frac{\partial T}{\partial X}+V\frac{\partial T}{\partial Y}\right]=\kappa\left[\frac{\partial^2 T}{\partial X^2}+\frac{\partial^2 T}{\partial Y^2}\right]-\frac{\partial q_r}{\partial Y}+(\rho c')_p D_B\left(\frac{\partial C}{\partial X}\frac{\partial T}{\partial X}+\frac{\partial C}{\partial Y}\frac{\partial T}{\partial Y}\right)$$
$$+(\rho c')_p\frac{D_T}{T_m}\left[\left(\frac{\partial T}{\partial X}\right)^2+\left(\frac{\partial T}{\partial Y}\right)^2\right]+\sigma' \mathrm{B}_0^2(U\cos\vartheta-V\sin\vartheta)^2, \tag{7}$$

$$\left[\frac{\partial C}{\partial t'}+U\frac{\partial C}{\partial X}+V\frac{\partial C}{\partial Y}\right]=D_B\left[\frac{\partial^2 C}{\partial X^2}+\frac{\partial^2 C}{\partial Y^2}\right]+\frac{D_T}{T_m}\left[\frac{\partial^2 C}{\partial X^2}+\frac{\partial^2 C}{\partial Y^2}\right], \tag{8}$$

where $U, V, \rho_f, \rho_p, t', T_m, P, T, C, D_B, D_T, S_{XX}, S_{XY}, S_{YX}, S_{YY}, q_r, \alpha, \sigma', B_0, \vartheta, \mu, c', \kappa$, g and k denote the components of velocity along X and Y direction respectively, density of fluid, density of particle, dimensional time, mean temperature of fluid, pressure, temperature of nanoparticle, nanoparticle concentration, Brownian diffusion coefficient, themophoretic diffusion coefficient, components of stress tensor, radiative heat flux, inclination angle of channel, electrical conductivity, uniform applied magnetic field, inclination angle of magnetic field, coefficient of viscosity of the fluid, volumetric volume expansion coefficient, thermal conductivity, acceleration due to gravity and permeable parameter. The radiative heat flux q_r is considered negligible in the X-direction when compared with Y- direction. Hence by using Rosseland approximation for radiation, the radiative heat flux is given by

$$q_r=\frac{16\sigma^* T_0^3}{3k^*}\frac{\partial T}{\partial Y}. \tag{9}$$

Where $\sigma^*$and k^* are the Stefan-Boltzmann constant and the mean absorption coefficient, respectively.
The extra stress tensor for pseudoplastic fluid [29] is given as follows:

$$\mathbf{S}+\lambda_1\frac{D\mathbf{S}}{Dt}+\frac{1}{2}(\lambda_1-\mu_1)(\mathbf{A}_1\mathbf{S}+\mathbf{S}\mathbf{A}_1)=\mu\mathbf{A}_1, \tag{10}$$

In which λ_1 and μ_1 are the relaxation times. Also

$$\mathbf{A}_1 = \nabla\mathbf{V} + (\nabla\mathbf{V})^T, \quad \frac{D\mathbf{S}}{Dt} = \frac{d\mathbf{S}}{dt} - (\nabla\mathbf{V}) - \mathbf{S}(\nabla\mathbf{V})^T.$$

The stress components S_{XX}, S_{XY} and S_{YY} can be obtained through the following relations:

$$S_{XX} + \lambda_1^*\left[\left(\frac{\partial}{\partial t'} + U\frac{\partial}{\partial X} + V\frac{\partial}{\partial Y}\right)S_{XX} - 2S_{XX}\frac{\partial U}{\partial X} - 2S_{XY}\frac{\partial U}{\partial Y}\right] + \frac{1}{2}(\lambda_1^* - \mu_1^*)\left[4S_{XX}\frac{\partial U}{\partial X} + 2S_{XY}\left(\frac{\partial U}{\partial Y} + \frac{\partial V}{\partial X}\right)\right] = 2\mu\frac{\partial U}{\partial X}, \tag{11}$$

$$S_{XY} + \lambda_1^*\left[\left(\frac{\partial}{\partial t'} + U\frac{\partial}{\partial X} + V\frac{\partial}{\partial Y}\right)S_{XY} - S_{XX}\frac{\partial V}{\partial X} - S_{YY}\frac{\partial U}{\partial Y}\right] \frac{1}{2}(\lambda_1^* - \mu_1^*)(S_{XX} + S_{YY})\left(\frac{\partial U}{\partial Y} + \frac{\partial V}{\partial X}\right) = \mu\left(\frac{\partial U}{\partial Y} + \frac{\partial V}{\partial X}\right), \tag{12}$$

$$S_{YY} + \lambda_1^*\left[\left(\frac{\partial}{\partial t'} + U\frac{\partial}{\partial X} + V\frac{\partial}{\partial Y}\right)S_{YY} - 2S_{YX}\frac{\partial V}{\partial X} - 2S_{YY}\frac{\partial V}{\partial Y}\right] \frac{1}{2}(\lambda_1^* - \mu_1^*)\left[2S_{YX}\left(\frac{\partial U}{\partial Y} + \frac{\partial V}{\partial X}\right) + 4S_{YY}\frac{\partial V}{\partial X}\right] = 2\mu\frac{\partial V}{\partial X}. \tag{13}$$

The appropriate boundary conditions comparising wall no-slip and convective boundary conditions are given as follows:

$$\mathrm{U} = 0, \ -k_h\frac{\partial T}{\partial Y} = h_h(T_0 - T) \text{ and } -k_m\frac{\partial C}{\partial Y} = h_m(C_0 - C) \text{ at } \mathrm{Y} = \mathrm{H}_1 \tag{14}$$

$$\mathrm{U} = 0, \ -k_h\frac{\partial T}{\partial Y} = h_h(T - T_1) \text{ and } -k_m\frac{\partial C}{\partial Y} = h_m(C - C_1) \text{ at } \mathrm{Y} = \mathrm{H}_2 \tag{15}$$

Where h_h and h_m are the heat and mass transfer coefficient, k_h is thermal conductivity and k_m is the mass diffusivity coefficients respectively.

We consider the following non-dimensional quantities:

$$x = \frac{X}{\lambda}, \ y = \frac{Y}{d}, \ t = \frac{ct'}{\lambda}, \ \mathrm{u} = \frac{U}{c}, \ v = \frac{V}{c}, \ \delta = \frac{d}{\lambda}, \ h_1 = \frac{H_1}{d}, \ h_2 = \frac{H_2}{d}, \ \theta = \frac{T - T_0}{T_1 - T_0}, \ \mathrm{p} = \frac{d^2P}{\lambda\mu c},$$

$$s_{ij} = \frac{d}{c\mu}S_{ij}, \ \lambda_1 = \frac{\lambda_1^* c}{d}, \ \mu_1 = \frac{\mu_1^* c}{d}, \ \sigma = \frac{C - C_0}{C_1 - C_0}, \ Re = \frac{\rho_f cd}{\mu}, \ B_m = \frac{h_m d}{k_m}, \ B_h = \frac{h_h d}{k_h}, \ a = \frac{a_1}{d},$$

$$b = \frac{a_2}{d}, \ m = \frac{m'\lambda}{d}, \ Pr = \frac{\mu c_f'}{k}, \ Nb = \frac{\tau D_B(C_1 - C_0)}{v}, \ Nt = \frac{\tau D_T(T_1 - T_0)}{T_m v}, \ M = \sqrt{\frac{\sigma'}{\mu}}dB_0, \ Rn = \frac{16\sigma^* T_0^3}{3k^*\mu c_f'},$$

$$\mathrm{Sc} = \frac{v}{D_B}, \ D_a = \frac{\kappa}{d^2}, \ Ec = \frac{c^2}{c_p(T_0 - T_1)}, \ Fr = \frac{c^2}{gd}, \ u = \frac{\partial\psi}{\partial y}, \ v = -\delta\frac{\partial\psi}{\partial x}. \tag{16}$$

Where ψ is the stream function.

Using the above dimensionless quantities, continuity equation is identically satisfied and Eqs. (5)-(8) become

$$Re\delta\left[\psi_y\psi_{xy} - \psi_x\psi_{yy}\right] = -\frac{\partial p}{\partial x} + \delta\frac{\partial}{\partial x}(s_{xx}) + \frac{\partial}{\partial y}(s_{xy}) - M^2\cos\vartheta(\psi_y\cos\vartheta + \delta\psi_x\sin\vartheta) - \frac{1}{D_a}\psi_y + \frac{Re\sin\alpha}{Fr}, \tag{17}$$

$$Re\delta^3\left[-\psi_y\psi_{xx} + \psi_x\psi_{xy}\right] = -\frac{\partial p}{\partial y} + \delta^2\frac{\partial}{\partial x}(s_{xy}) + \delta\frac{\partial}{\partial y}(s_{yy}) - \frac{\delta^2}{D_a}v + M^2\delta\sin\vartheta(u\cos\vartheta - v\sin\vartheta) - \delta\frac{Re\sin\alpha}{Fr}, \tag{18}$$

$$Re\delta\left[\frac{\partial\theta}{\partial t} + \psi_y\frac{\partial\theta}{\partial x} - \psi_x\frac{\partial\theta}{\partial y}\right] = \frac{1}{Pr}\left[\delta^2\frac{\partial^2\theta}{\partial x^2} + \frac{\partial^2\theta}{\partial y^2}\right] + Rn\left(\frac{\partial^2\theta}{\partial y^2}\right) + Nb\left[\delta^2\frac{\partial\sigma}{\partial x}\frac{\partial\theta}{\partial x} + \frac{\partial\sigma}{\partial y}\frac{\partial\theta}{\partial y}\right]$$

$$+ Nt\left[\delta^2\left(\frac{\partial\theta}{\partial x}\right)^2 + \left(\frac{\partial\theta}{\partial y}\right)^2\right] + Ec.M^2\left(\cos^2\vartheta(\psi_y)^2 - \delta^2\sin^2\vartheta(\psi_x)^2 - \delta\psi_y\psi_x\sin\vartheta\cos\vartheta\right), \tag{19}$$

$$Re\delta.Sc\left[\frac{\partial\sigma}{\partial t}+\psi_y\frac{\partial\sigma}{\partial x}-\psi_x\frac{\partial\sigma}{\partial y}\right]=\delta^2\frac{\partial^2\sigma}{\partial x^2}+\frac{\partial^2\sigma}{\partial y^2}+\frac{N_t}{Nb}\left[\delta^2\frac{\partial^2\theta}{\partial x^2}+\frac{\partial^2\theta}{\partial y^2}\right]. \quad (20)$$

With non-dimensional stress components are:

$$s_{xx}+\lambda_1\left[\delta\left(\frac{\partial}{\partial t}+\psi_y\frac{\partial}{\partial x}-\psi_x\frac{\partial}{\partial y}\right)s_{xx}-2\delta s_{xx}\psi_{xy}-2s_{xy}\psi_{yy}\right]+\frac{1}{2}(\lambda_1-\mu_1)\left[4\delta s_{xx}\psi_{xy}+2s_{xy}(\psi_{yy}-\delta^2\psi_{xx})\right]=2\delta\psi_{xy}, \quad (21)$$

$$s_{xy}+\lambda_1\left[\delta\left(\frac{\partial}{\partial t}+\psi_y\frac{\partial}{\partial x}-\psi_x\frac{\partial}{\partial y}\right)s_{xy}+\delta^2 s_{xx}\psi_{xx}-s_{xy}\psi_{yy}\right]+\frac{1}{2}(\lambda_1-\mu_1)\left[(s_{xx}+s_{yy})(\psi_{yy}-\delta^2\psi_{xx})\right]=\psi_{yy}-\delta^2\psi_{xx}, \quad (22)$$

$$s_{yy}+\lambda_1\left[\delta\left(\frac{\partial}{\partial t}+\psi_y\frac{\partial}{\partial x}-\psi_x\frac{\partial}{\partial y}\right)s_{yy}+2\delta s_{yy}\psi_{xy}-2\delta^2 s_{xy}\psi_{xx}\right]+\frac{1}{2}(\lambda_1-\mu_1)\left[-4\delta s_{yy}\psi_{xy}+2s_{xy}(\psi_{yy}-\delta^2\psi_{xy})\right]=-2\delta\psi_{xy}, \quad (23)$$

Similarly Eqs. (14) and (15) become

$$\psi_y=0,\ \theta_y=B_h\theta \text{ and } \sigma_y=B_m\sigma \text{ at } y=h_1, \quad (24)$$

$$\psi_y=0,\ \theta_y=B_h(1-\theta) \text{ and } \sigma_y=B_m(1-\sigma) \text{ at } y=h_2. \quad (25)$$

where x is the non-dimensional axial coordinate, y is the non-di mensional transverse coordinate, t is the dimensionless time, u and v are non-dimensional axial and transverse velocity components re spectively, p is the dimensionless pressure, a and b are amplitudes of upper and lower walls, δ is the wave number, m is the non- uniform parameter, R is the Reynolds number, v is the nanofluid kinematic viscosity, τ is the ratio of the effective heat capacity of nanoparticle material and heat capacity of the fluid, θ is the dimensionless temperature, σ is the dimensionless rescaled nanoparticle volume fraction, Pr is the Prandtl number, E_c is the Eckert number, S_c is the Schmidt number,M is the Hartmann number, permeability parameter D_a, $B_r = E_c.P_r$ is the Brinkman number, Nb is the Brownian motion parameter, Nt is the thermophoresis parameter, Rn is the thermal radiation parameter, B_h and B_m the heat and mass transfer Biot numbers respectively,and F_r is the Froude number.

Introducing the wave frame having coordinates (X,Y) travelling in the X-direction with same wave velocity c. The velocities and coordinates in two frames are related by

$$X=\bar{X}-ct,\ Y=\bar{Y},\ U=\bar{U}-c,\ V=\bar{V}. \quad (26)$$

Eqs.(17)-(23) under long wavelength and low Reynolds number approximation lead to following set of equations:

$$\frac{\partial p}{\partial x}=\frac{\partial x}{\partial x}(s_{xy})-M^2\cos^2\vartheta\psi_y-\frac{1}{Da}\psi_y+\frac{Re\sin\alpha}{Fr}, \quad (27)$$

$$\frac{\partial p}{\partial y}=0, \quad (28)$$

$$(1+PrRn)\frac{\partial^2\theta}{\partial y^2}NbPr\left(\frac{\partial\sigma}{\partial y}\frac{\partial\theta}{\partial y}\right)NtPr\left(\frac{\partial\theta}{\partial y}\right)^2+BrM^2\cos^2\vartheta(\psi_y)^2=0, \quad (29)$$

$$\frac{\partial^2\sigma}{\partial y^2}+\frac{N_t}{Nb}\frac{\partial^2\theta}{\partial y^2}=0. \quad (30)$$

With

$$s_{xx}=(\lambda_1-\mu_1)s_{xy}\psi_{yy}, \quad (31)$$

$$s_{xy}+\frac{1}{2}(\lambda_1-\mu_1)(s_{xx}+s_{yy})\psi_{yy}-\lambda_1 s_{yy}\psi_{yy}=\psi_{yy}, \quad (32)$$

$$s_{yy}=-(\lambda_1-\mu_1)\mathrm{s}_{\mathrm{xy}}\psi_{yy}. \quad (33)$$

Eliminating pressure from Eqs. (27) and (28) and simplifying Eqs. (31)-(33), we get the following system:

$$\frac{\partial^2}{\partial y^2}(sxy)-M^2\cos^2\vartheta\psi_{yy}-\frac{1}{Da}\psi_{yy}=0 \quad (34)$$

Substituting Eqs. (31) and (33) into Eq. (32) we have

$$sxy=\frac{\psi_{yy}}{1-\xi(\psi_{yy})^2}, \quad (35)$$

The appropriate boundary conditions of this problem are given below

$$\psi=-\frac{F}{2},\ \psi_y=0,\ \theta_y=B_h\theta \text{ and } \sigma_y=B_m\sigma \text{ at } y=h_1=-1-mx-a\sin[2\pi(x-t)+\phi], \quad (36)$$

$$\psi=\frac{F}{2},\ \psi_y=0,\ \theta_y=B_h(1-\theta) \text{ and } \sigma_y=B_m(1-\sigma) \text{ at } y=h_2=1+mx+b\sin[2\pi(x-t)] \quad (37)$$

Here $\xi=(\mu_1^2-\lambda_1^2)$ is the pseudoplastic fluid parameter

and F denotes the non-dimentional mean flows.

3. Rate of Volume Flow

In laboratory frame, the dimensional volume flow rate is

$$Q(X,t)=\int_{H_1(X,t)}^{H_2(X,t)}U(X,Y,\mathrm{t})\,\mathrm{dY}, \tag{38}$$

In which H_1 and H_2 are functions of X and t.
In wave frame, the dimensional volume flow rate is

$$\mathrm{q}=\int_{H_1}^{H_2}\bar{U}(\bar{X},\bar{\mathrm{Y}})\,\mathrm{d}\bar{\mathrm{Y}}, \tag{39}$$

Substituting Eq. (26) in Eq. (38), we obtain

$$Q(X,t)=q+cH_1-cH_2. \tag{40}$$

The time averaged flow at afixed position $\bar{X}$ over a period ($T=\lambda/\mathrm{c}$) is defined as

$$\bar{Q}=\frac{1}{T}\int_0^T Q dt. \tag{41}$$

If we substitute Eq. (39) into Eq. (40) and integrating, we get

$$\bar{Q}=q+a_1c\sin\frac{2\pi}{\lambda}(X-ct)+a_2c\sin\left[\frac{2\pi}{\lambda}(X-ct)+\phi\right]. \tag{42}$$

If we find the dimensionless mean flows F, in the laboratorty frame, and Θ, in the wave frame, according to

$$F=\frac{\bar{Q}}{cd},\quad \Theta=\frac{q}{cd},$$

One can find thet Eq. (42) becomes

$$F(x,t)=\Theta+a\sin[2\pi(x-t)]+b\sin[2\pi(x-t)+\phi]. \tag{43}$$

In which

$$F=\int_{h_1}^{h_2}u\ dy\,. \tag{44}$$

The coefficient of heat transfer at the right wall is given by

$$Z=h_{1x}(\theta_y)_{y=h1}, \tag{45}$$

The pressure rise per wavelength is given by

$$\Delta p=\int_0^1\int_0^1\left(\frac{\partial p}{\partial x}\right)_{y=0}dxdt. \tag{46}$$

The system of coupled equations (29), (30) and (34) subject to the boundary conditions (36) and (37) is solved numerically for stream function, temperature distribution, nanoparticle volume fraction and pressure gradient component by using the built-in command NDSolve in Mathematica. The coefficient of heat transfer and pressure rise per wavelength are computed in a similar manner.

4. Results and Discussion

This section deal with the graphical description of various parameters on the flow of pseudoplastic nanofluids in the inclined tapered asymmetric channel. Particularly the results of average pressure rise, axial velocity, temperature distribution, streamlines and heat transfer coefficient are recorded in terms of plot and then discussed physically.

4.1. Pumping Characteristics

Figs. 2-8 are the graph of the dimensionless average rise in pressure against the variation of mean flow rate Θ. The expression for Δp involves the integration of dp/dx. Due to complexity of dp/dx Eq. (46) is not itegrable analytically. Consequently, a numerical integration scheme required for the evaluation of the integrals. MATHEMATICA and MATLAB are used to evaluate the integrals and all the plots have been then generated for the various values of the parameters of interest. Figs. 2-4 shows the impact of b,a and M on average pressure rise Δp. It can be seen from the graphs that in co-pumping region ($\Delta p < 0$, $\Theta > 0$), the pumping rate decreases with an increase in b,a and M. Effect of ϑ on Δp is sketched in Fig. 5. It is observed that in backward pumping region or retrograde ($\Delta p > 0$, $\Theta < 0$), the pumping rate decreases with an increase in ϑ, while in co-pumping region ($\Delta p < 0$, $\Theta > 0$) the pumping increases via ϑ. Average pressure rise Δp for various values of ϕ is plotted in Fig. 6. graph shows that the pumping rate decreases in the co-pumping region $\Delta p < 0$, while in the retrograde ($\Delta p > 0$, $\Theta < 0$) and free pumping region $\Delta p = 0$ enhances with an increase in ϕ. Fig. 7. shows the impact of m on pressure rise Δp. It is observed that in co-pumping region ($\Delta p < 0$, $\Theta > 0$), the pumping rate decreases with an increase in m. Fig. 8 shows the variation of average rise in pressure against mean flow rate Θ, for different values of D_a. IT is noticed that the pumping rate decreases with an increase in D_a and in co-pumping, the pumping rate increases with an increase in D_a.

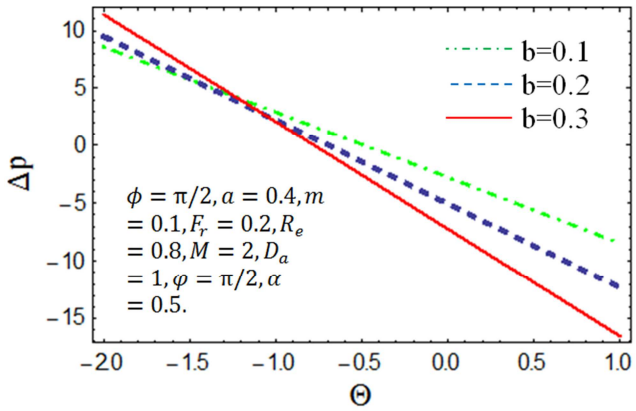

Fig. 2. *Pressure rise for variation of b.*

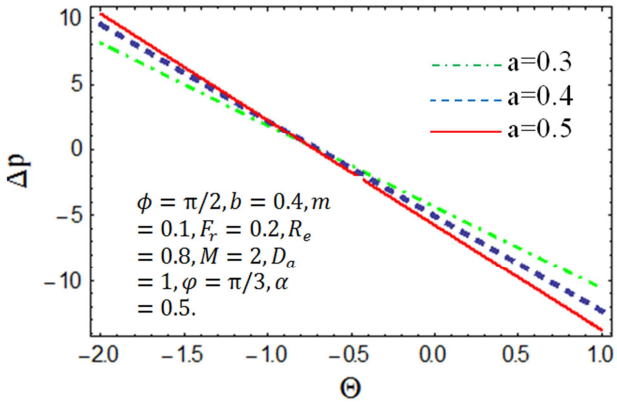

Fig. 3. *Pressure rise for variation of a.*

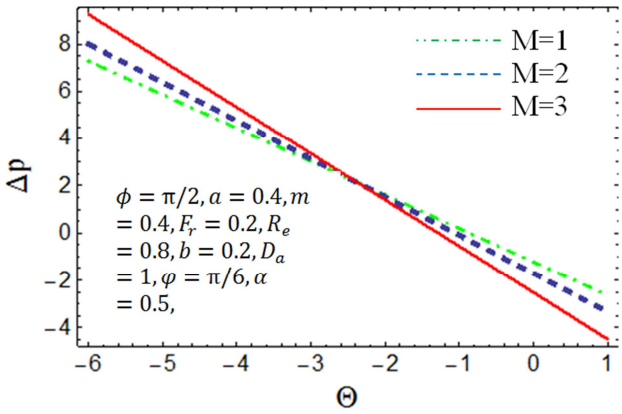

Fig. 4. *Pressure rise for variation of M.*

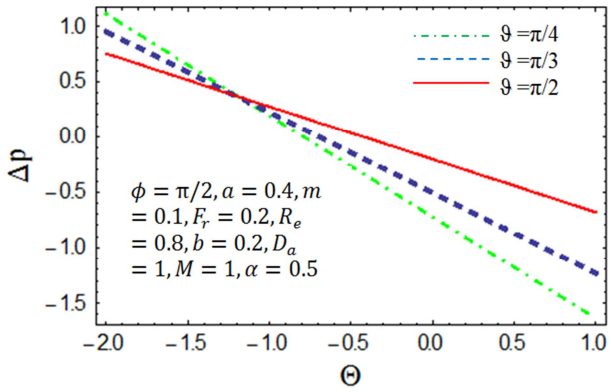

Fig. 5. *Pressure rise for variation of ϑ.*

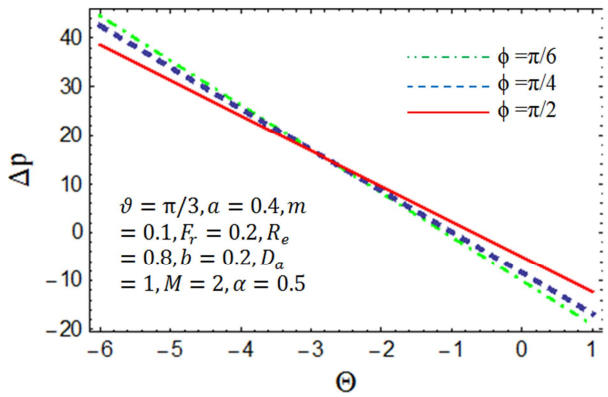

Fig. 6. *Pressure rise for variation of ϕ.*

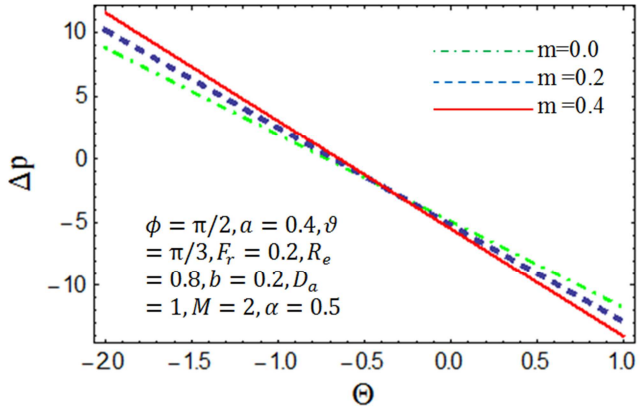

Fig. 7. *Pressure rise for variation of m.*

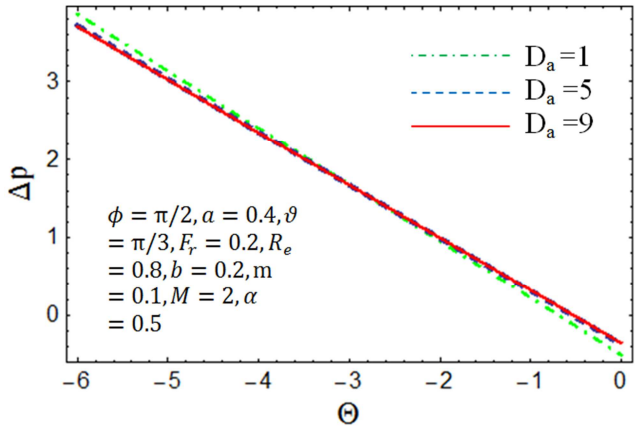

Fig. 8. *Pressure rise for variation of D_a.*

4.2. Velocity Profile

Figs. 9-14 skrtched at the fixed values of *x=0.3*, *t=0.1* such that display the effects of various physical parameters on the velocity profile *u(y)*. Fig. 9 depicts that the velocity profile for *m*. We observed that the axial velocity *u* decreases with an increase in *m* at the core part of the channel. Fig. 10 shows the effect of *b* on the velocity profile. It is observed that increasing *b* results in a decrease in the velocity profile. But the velocity increase after *y=0.29* whith an increase in *b*. .11 shows the influence of *Θ* on the axial velocity. It is observed that the axial velocity profile increases with an increase in *Θ*. Effect of *M* on the axial velocity is plotted in Fig. 12. It is seen that increasing *M* causes the velocity pofile to decrease at the core of channel whereas increasing behavior is noticed near the walls of channel. The axial velocity profile for the *ξ* is plotted in Fig. 13. It is seen that the velocity profile is not symmetric and the velocity decreases after *y=-0.55* with an increase in *ξ*. Fig. 14 displays the influence of *ϕ* on the axial velocity distribution. It reveals that an increase in *ϕ* causes the velocity profile to increase at the core of channel whereas decreasing behavior is noticed near the walls of channel.

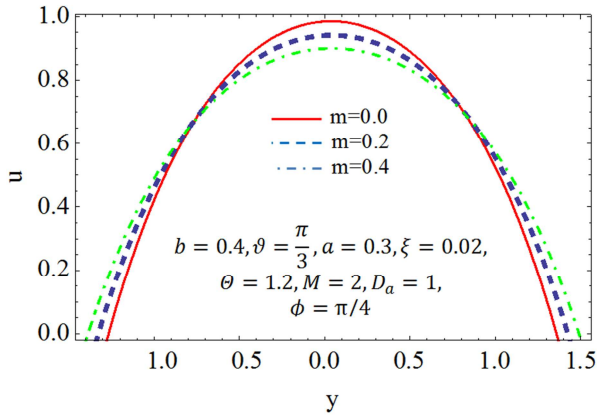

Fig. 9. *Axial velocity for m.*

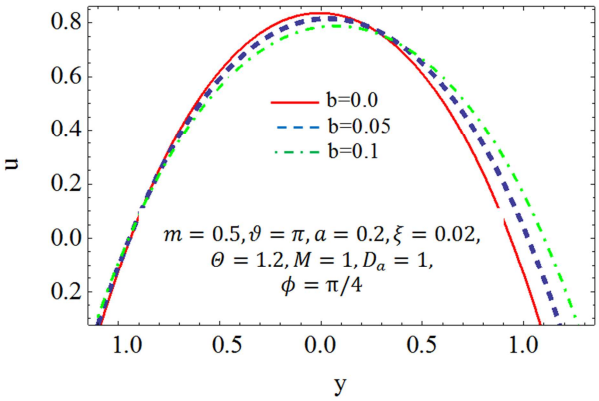

Fig. 10. *Axial velocity for b.*

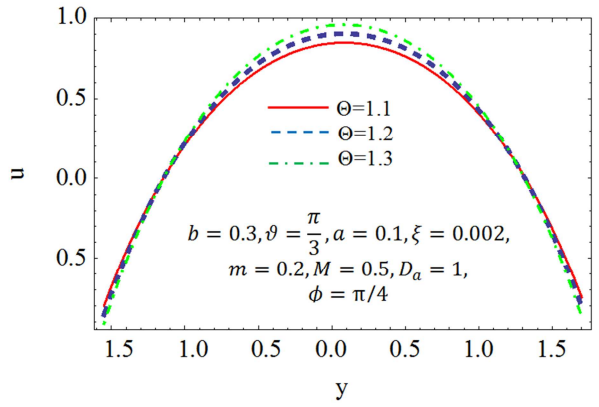

Fig. 11. *Axial velocity for Θ.*

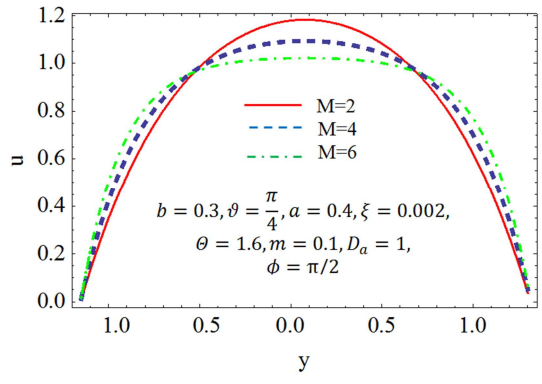

Fig. 12. *Axial velocity for M.*

4.3. Temperature Distribution

Figs. 15-20 have been plotted to analyze the impact of mass transfer Biot number B_m, heat transfer Biot number B_h, Brownian motion parameter N_b, thermophoresis parameter N_t, Prandtl number P_r and inclination angle ϕ of magnetic field. Figs. 15 and 18 shows dual behavior of temperature with an increase in B_m and N_t, i.e., large values of B_m and N_t enhances fluid temperature near left wall of channel since increase in B_m and N_t enhances transfer of heat. However near the right channel wall increase in B_m and N_t reduces thermal conductivity more efficiently which causes reduction of temperature. The temperature distribution for B_h and ϕ are plotted in Fig. 16 and 20. It is seen that the temperature profile enhances with an increase in B_h and ϕ. Figs. 17 and 19 shows dual behavior of temperature with an increase in N_b and P_r, i.e., larger values of N_b and P_r enhances fluid temperature near right wall of the channel since increase in N_b and P_r enhances transfer of heat. However near the left channel wall increase in N_b and P_r reduces thermal conductivity more efficiently which causes reduction of temperature.

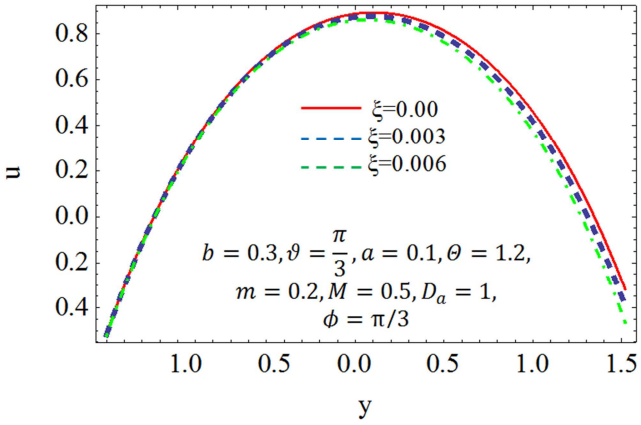

Fig. 13. *Axial velocity for ξ.*

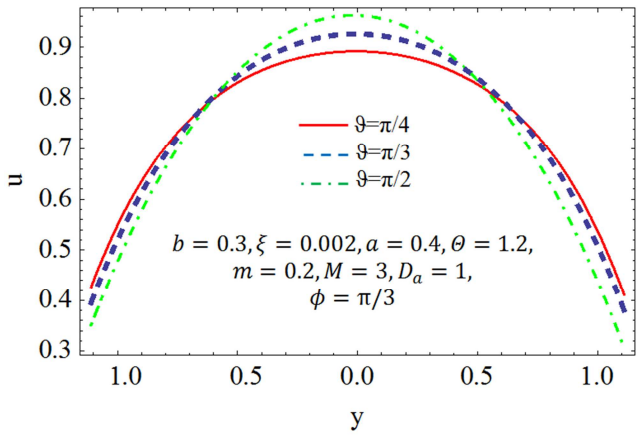

Fig. 14. *Axial velocity for ϑ.*

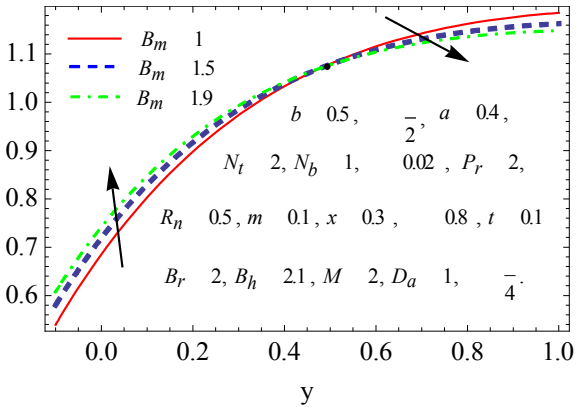

Fig. 15. *Temperature distribution of B_m.*

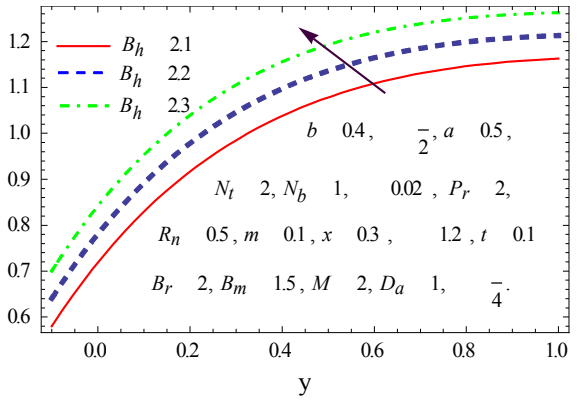

Fig. 16. *Temperature distribution of B_h.*

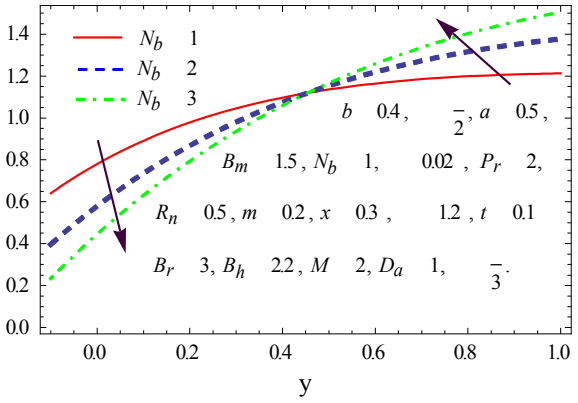

Fig. 17. *Temperature distribution of N_b.*

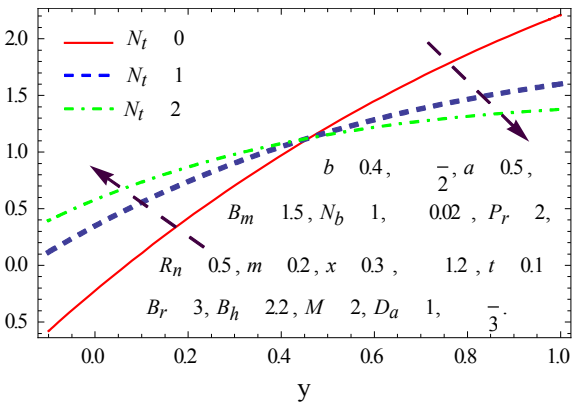

Fig. 18. *Temperature distribution of N_t.*

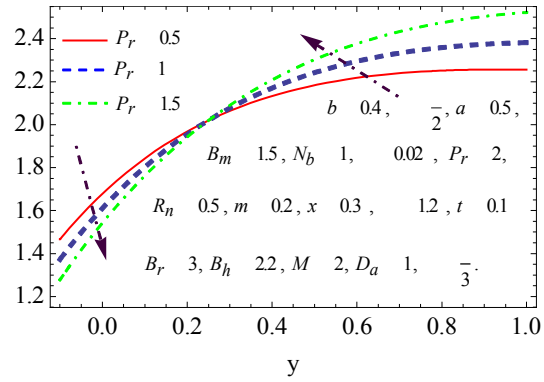

Fig. 19. *Temperature distribution of P_r.*

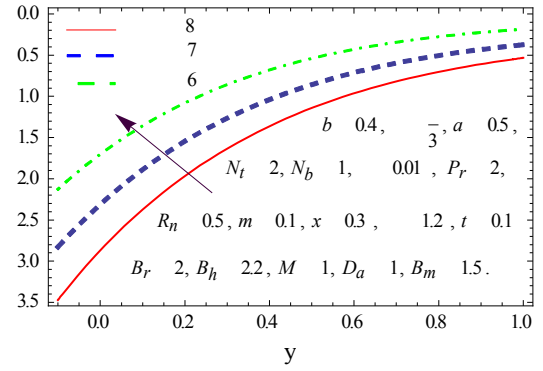

Fig. 20. *Temperature distribution of 9.*

4.4. Heat Transfer Coefficient

In Figs. 21-27 the variation of heat transfer coefficient *Z(x)* for variations values of emrging parameters is analyzed. The heat transfer coeficient is denoted by $Z(x)=h_{1x}\theta_y(h_1)$ which actually defines the rate of heat transfer or heat flux at the lower wall. It is found that the nature of heat transfer cofficient is oscillatory. This is expected due to propagation 0f sinusoidal waves along the channel walls. Figs. 21 and 25 shows that absolute value of Z decreases with an increase in B_h and ξ. However greator impact is noticed near $0.2 < x < 0.7$. Figs. 23 shows that absolute value of Z increases with an increase in N_b. Figs 22 and 24 signifies the decreasing response of absolute heat transfer coefficient Z with an increase in R_n and Nt. More clear results are noticed in the range where $0.2 < x < 0.7$. Figs. 26 drawn to explain that absolute value of Z decreases with an increase in m.

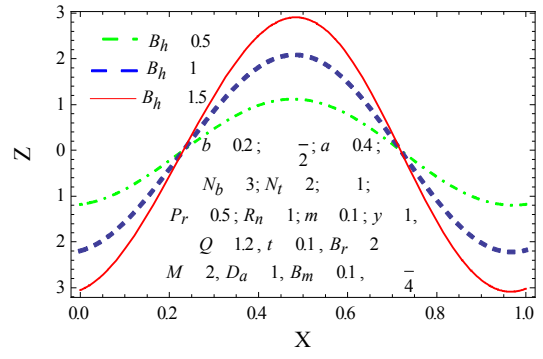

Fig. 21. *Heat transfer coefficient for B_h.*

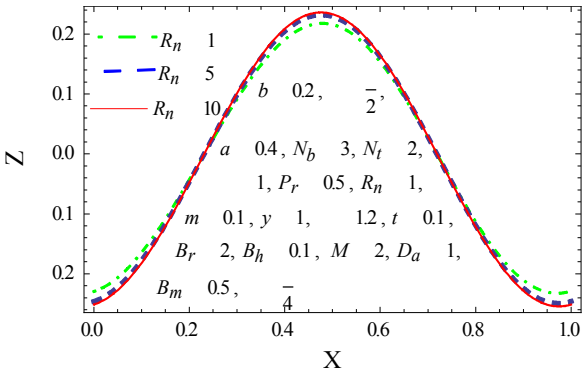

Fig. 22. *Heat transfer coefficient for R_n.*

4.5. Trapping

Another interesting phenomenon in peristaltic motion is trapping. In the wave frame, streamlines under certain conditions split to trap a bolus which moves as a whole with the speed of the wave. The trapping for different values of b, ϕ, a, D_a, ξ, ϑ and m are showen in Figs. 28-35 at fixed values of $t = 0.4$. It is interesting to notice that bolus appears only near the upper wall in all cases. Fig. 27 displays the influence of amplitude of upper wall on the streamlines. We note that the trapping bolus increase with increasing b. In Fig. 28 we observe that the trapped bolus increases in size as ϑ increases and more trapped bolus appears near the lower wall with increasing ϑ. Fig. 29 effect of amplitude of lower wall on the streamlines. We note that the trapping bolus increases with increasing in a. Fig. 30 show that the bolous is vanish when there is an increase in Hartman number M. The influence of Darcy number D_a on the streamlines is displayed in Fig. 31. We observe that the trapped bolus increases in size as D_a increases and more trapped bolus appears with increasing D_a. Fig. 32 depicts that ψ increases by increasing Θ. Fig. 33 shows the streamlines pattern for different values of the inclination angle of the channel ϕ. We observed that the size of trapped bolus decreases by increasing ϕ. The effects of uniform and non-uniform channels m on the trapping are shown in Fig. s34. It is examined that the size of bolus is symmetric and appears in the same size on the lower wall of the channel while in the non-uniform channel, we observed that bolus become bigger when it has different size an the lower wall of tapered asymmetric channel.

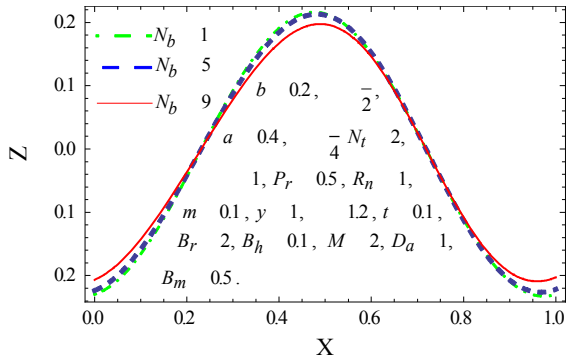

Fig. 23. *Heat transfer coefficient for N_b.*

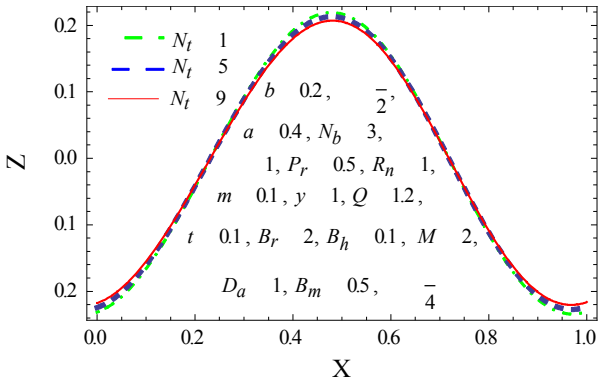

Fig. 24. *Heat transfer coefficient for N_t.*

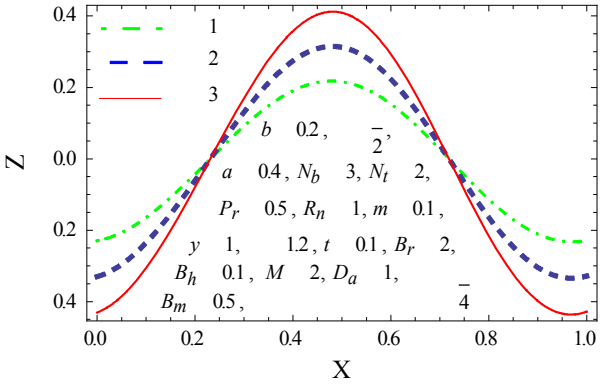

Fig. 25. *Heat transfer coefficient for ξ.*

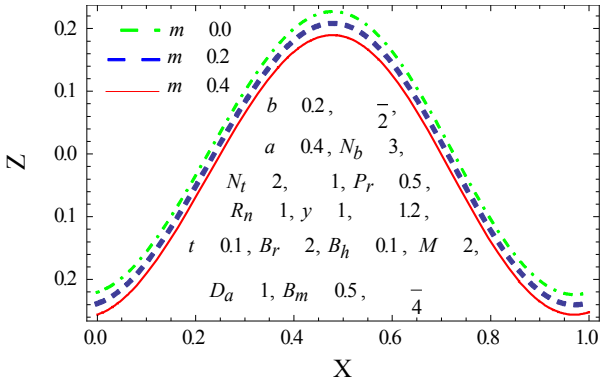

Fig.26. *Heat transfer coefficient for m*

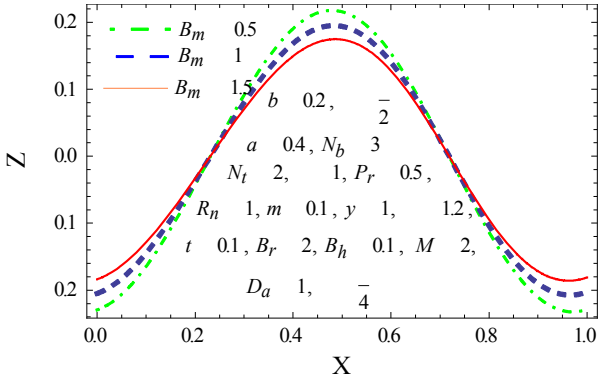

Fig. 27. *Heat transfer coefficient for B_m.*

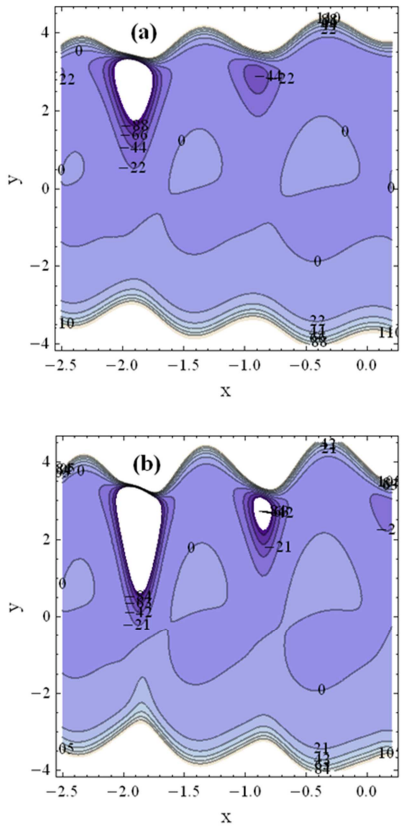

Fig. 28. *Streamlines when a=0.2, ϑ=π/3, M=1, D_a=1, ξ=0.01, t=0.4, Θ=1.2, ϕ=π/4, m=0.1. (a) b=0.3 and (b) b=0.5.*

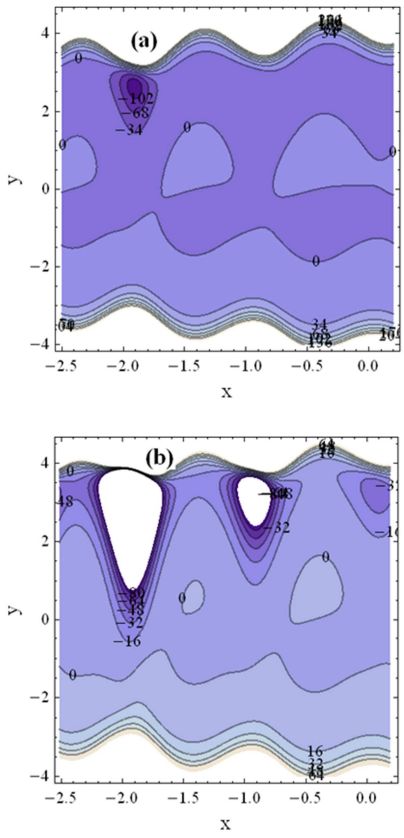

Fig. 29. *Streamlines when a=0.2, b=0.3, M=1, D_a=1, ξ=0.01, t=0.4, Θ=1.2, ϕ=π/4, m=0.1. (a) ϑ=π/4 and (b) ϑ=π/2.*

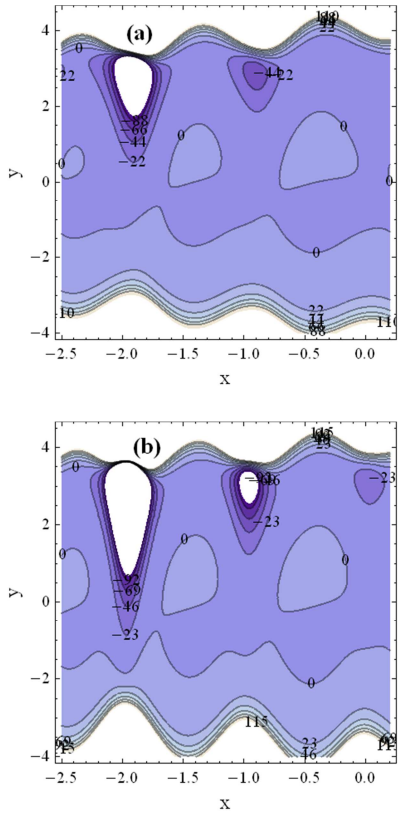

Fig. 30. *Streamlines when D_a=1, ϑ=π/3,Θ=1.2, b=0.3, M=1, ξ=0.01, t=0.4, ϕ=π/4, m=0.1. (a) a=0.2 and (b) a=0.4.*

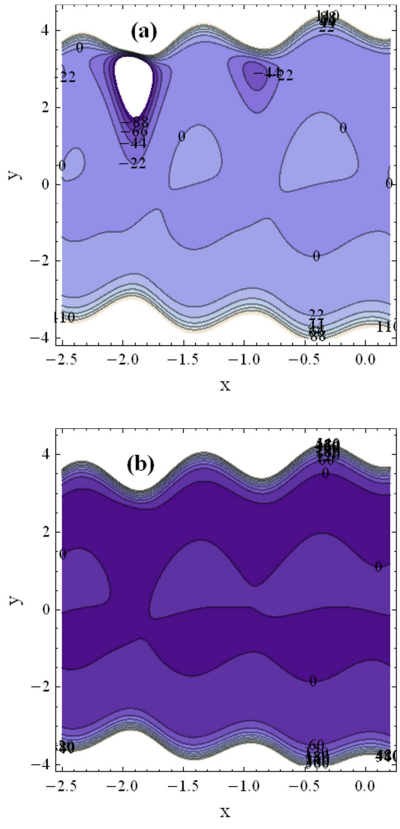

Fig. 31. *Streamlines when D_a=1, ϑ=π/3, a=0.2, b=0.3, Θ=1.2, ξ=0.01, t=0.4, ϕ=π/4, m=0.1. (a) M=1 and (b) M=2.*

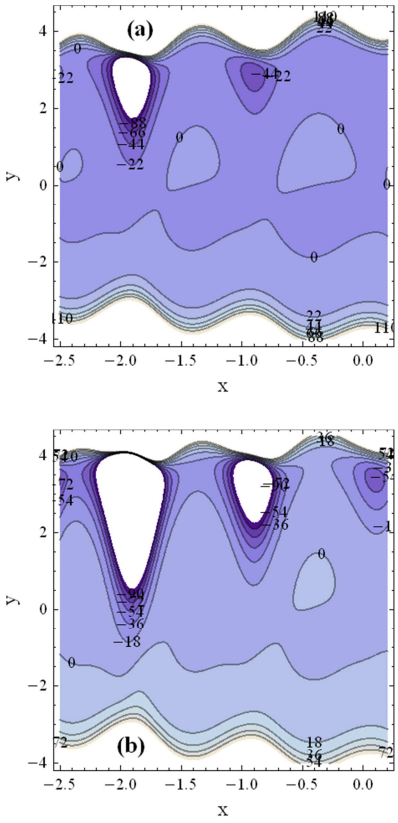

Fig. 32. *Streamlines when $\vartheta=\pi/3$, $a=0.2$, $b=0.3$, $M=1$, $\xi=0.01$, $t=0.4$, $\Theta=1.2$, $\phi=\pi/4$, $m=0.1$. (a) $D_a=1$ and (b) $D_a=1.5$.*

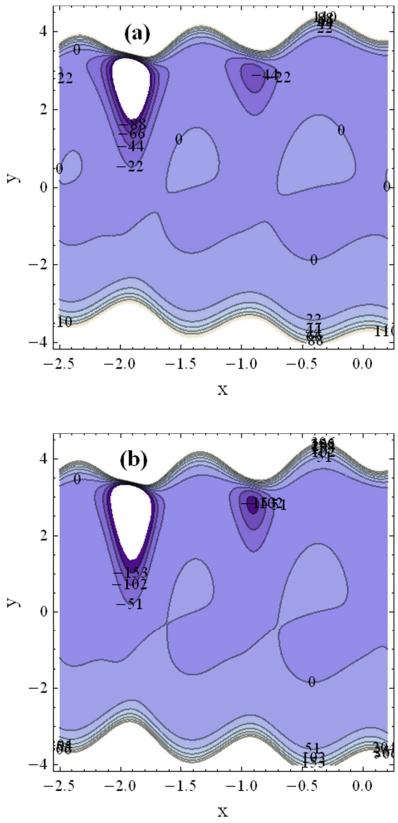

Fig. 33. *Streamlines when $D_a=1$, $\vartheta=\pi/3$, $a=0.2$, $b=0.3$, $M=1$, $\xi=0.01$, $t=0.4$, $\phi=\pi/4$, $m=0.1$. (a) $\Theta=1.2$ and (b) $\Theta=1.6$.*

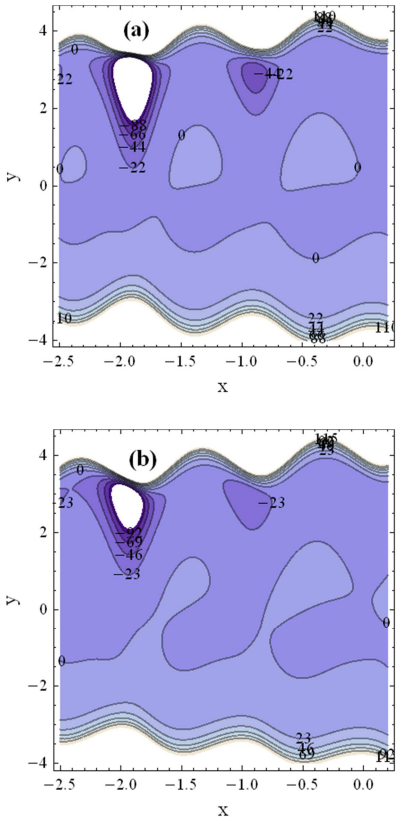

Fig. 34. *Streamlines when $\vartheta=\pi/3$, $a=0.2$, $b=0.3$, $M=1$, $D_a=1$, $t=0.4$, $\Theta=1.2$, $\xi=0.01$, $m=0.1$. (a) $\phi=\pi/6$ and (b). $\phi=\pi/2$.*

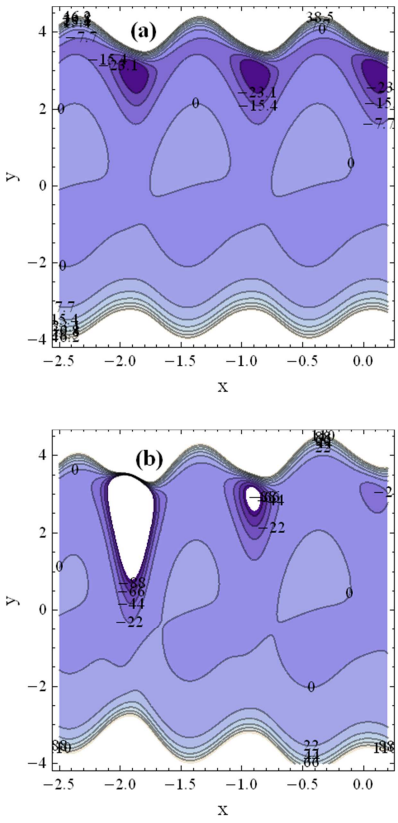

Fig. 35. *Streamlines when $\vartheta=\pi/3$, $a=0.2$, $b=0.3$, $M=1$, $D_a=1$, $t=0.4$, $\Theta=1.2$, $\phi=\pi/4$, $\xi=0.02$. (a) $m=0.0$ and (b) $m=0.1$.*

5. Concluding Remarks

In this paper we succeeded in presenting a mathematical model to study the peristaltic transport of pseudoplastic naonfluid through a porous mediam in an inclined tapered asymmetric channel. A regular perturbation method is employed to obtain the expression for the stream function, axial velocity, temperature, heat transfer coefficient and pressure rise over a wavelength. The interaction of the rheological parameters of the fluid with peristaltic flow is discussed. The main results can be summarized of follows :

- The pressure rise over a wavelength Δp decreases with an increase in M co-pumping region, while the situation is reserved in the pumping region.
- The pressure rise over a wavelength Δp decreases in the pumping rate with an increase in ϑ, while in co-pumping region the pumping increasesvia ϑ.
- The pumping reate decreases in the co-pumping region,while in the retrograde and free pumping region enhances with an increase in ϕ.
- In the co-pumping region, the pumping rate decreases with an increase in m.
- The pumping rate decreases with an increase in D_a and in co-pumping, the pumping rate increase with an increase in D_a.
- The axial velocity increases with increasing Θ, ϕ, and b while it decreases with increasing m, M and ξ.
- The temperature distribution has dual behavior with an increase in B_m, N_t, N_b and P_r.
- The trapping bolus increases with increasing a, b, ϕ and D_a while it decreases with increasing ξ and ϑ.
- Heat transfer coefficient $Z(x)$ increases for N_b.
- The trapped bolus is symmetric and appears in the same size on the lower wall of the inclined channel while it has a reverse behavior for non-uniform inclined channel.

References

[1] T. W. Latham, Fluid motion in a peristaltic pump, MS Thesis, MiT, USA, 1966.

[2] Y. C Fung, C. S. Yih, Peristaltic transport, ASME J, APPl. Mech. 35 (1968) 669-675.

[3] C. Barton, S Raynor, Peristaltic flow in tubes, Bull. Math. Biophys. 30 (1968) 663-680.

[4] A. H Shapiro, M. Y. Jafferin, S. l. Weinberg, Peristaltic pumping with long wavelength at low Reynolds number, J. Fluid Mech. 37 (1969) 799-825.

[5] A. M. Abd-Alla, S. M. Abo-Dahab, A. Kilicman, Peristaltic flow of aJeffrey fluid under the effect of radially varying magnetic field in a tube with an endoscope, J. Magn. Magn. Mater. 384 (2015) 79–86.

[6] A. M. Abd-Alla, S. M. Abo-Dahab, H. D. El-Shahrany, Effects of rotation and initial stress on peristaltic transport of fourth grade fluid with heat transfer and induced magnetic field, J. Magn. Mater. 349 (2014) 268–280.

[7] K. Nowar, Peristaltic flow of a nanofluid under the effect of Hall current and porous medium, Math. Prob. Eng (2014).

[8] M. Kothandapani, J. Prakash, Effect of radiation and magnetic field on peristaltic transport of nanofluids through a porous space in a tapered asymmetric channel, J. Magn. Magn. Mater. 378 (2015) 152–163.

[9] G. Radhakrishnamacharya, Ch. Srinivasulu, Influence of wall properties on peristaltic transport with heat transfer, C. R. Mec. 335 (2007) 369–373.

[10] S. Srinivas, M. Kothandapani, The influence of heat and mass transfer on MHD peristaltic flow through aporous space with compliant walls, Appl. Math. Comput. 213 (2009) 197–208.

[11] A. A. Shaaban, Mohamed Y. Abou-Zeid, Effects of heat and mass transfer on MHD peristaltic flow of a non-Newtonian fluid through a porous medium between two coaxial cylinders, Math. Prob. Eng. (2013).

[12] M. Kothandapani, J. Prakash, Influence of hea tsource, thermal radiation, and inclined magnetic field on peristaltic flow of a hyperbolic tangent nanofluid in a tapered asymmetric channel, IEEE Trans. Nanobiosci. 14 (2015) 385–392.

[13] H. Yasmin, T. Hayat, N. Alotaib, H. Gao, Convective heat and mass transfer analysis on peristaltic flow of Williamson fluid with Hall effects and Joule heating, Int. J. Biomath. (2014), http://dx.doi.org/10.1142/S1793524514500582.

[14] M. Kothandapani, J. Prakash, Convective boundary conditions effect on peristaltic flow of a MHD Jeffrey nanofluid, Appl. Nanosci. (2015), http://dx.doi.org/10.1007/ s13204-015-0431-9.

[15] R. Ellahi, M. M. Bhatti, K. Vafai, Effects of heat and mass transfer on peristaltic flow in a non-uniform rectangular duct, Int. J. Heat Mass Transf. 71 (2014) 706–719.

[16] T.Hayat, F. M. Abbasi, Maryem Al-Yami, Shatha Monaquel, Slip and Joule heating effects in mixed convection peristaltic transport of nanofluid with Soret and Dufour effects, J. Mol. Liq. 194 (2014) 93–99.

[17] M. Mustafa, S. Abbasbandy, S.Hina, T.Hayat, Numerical investigation on mixed convective peristaltic flow of fourth grade fluid with Dufour and Soret effect, J. Taiwan Inst. Chem. Eng. 45 (2014) 308–316.

[18] F. M. Abbasi, T. Hayat, A. Alsaedi, B. Ahmed, Soret and Dufour effects on peristaltic transport of MHD fluid with variable viscosity, Appl. Math. Inf. Sci. 8 (2014) 211–219.

[19] M. Kothandapani, J. Prakash, Effects of thermal radiation parameter and magnetic field on the peristaltic motion of Williamson nanofluids in a tapered asymmetric channel, Int. J. Heat Mass Transf. 81 (2015) 234–245.

[20] Obaid Ullah Mehmood, N. Mustapha, S. Shafie, T. Hayat, Partial slip effect on heat and mass transfer of MHD peristaltic transport in a porous medium, Sains Malays. 43 (2014) 1109–1118.

[21] S.U.S. Choi, Enhancing thermal conductivity of fluid with nanoparticles de velopments and applications of non-Newtonian flow, In: ASMEFED, vol. 66, 1995, pp. 99–105.

[22] D. Tripathi, O. A. Beg, Astudy on peristaltic flow of nanofluids: applicationin drug delivery systems, Int. J. Heat Mass Transf. 70 (2014) 61–70.

[23] S. A. Shehzad, F. M. Abbasi, T. Hayat, F. Alsaedi, Model and comparative study for peristaltic transport of water based nanofluids, J. Mol. Liq. 9 (2015) 723–728.

[24] F. M. Abbasi, S. A. Shehzad, T. Hayat, F. E. Alsaadi, Impact of magnetic field on mixed convective peristaltic flow of water based nanofluids with Joule heat ing, Z. Naturforsch. A 70 (2014) 125–132.

[25] S. Hina, M. Mustafa, T. Hayat, N. D. Alotaibid, On peristaltic motion of pseudoplastic fluid in a curved channel with heat/mass transfer and wall properties, Appl. Math. Comput. 263 (2015) 378–391.

[26] T. Hayat, A. Tanveer, F. Alsaadi, G. Mousa, Impact of radial magnetic field on peristalsis incurved channel with convective boundary conditions, J. Magn. Magn. Mater. 403 (2016) 47–59.

[27] T. Hayat, R. Iqbal, A.Tanveer, A. Alsaedi, Influence of convective conditions in radiative peristaltic flow of pseudoplastic nanofluid in a tapered asymmetric channel, J. Magn. Magn. Mater. 408 (2016) 168-176.